A droplet microfluidic-based sensor for simultaneous in situ monitoring of nitrate and nitrite in natural waters

Adrian M. Nightingale,[a] Sammer-ul Hassan,[a] Brett M. Warren,[b] Kyriacos Makris,[b] Gareth W. H. Evans,[a] Evanthia Papadopoulou,[b] Sharon Coleman,[a,b] and Xize Niu[a,b]*

[a]Mechanical Engineering, Faculty of Engineering and Physical Sciences, University of Southampton, Southampton, SO17 1BJ, United Kingdom.

[b]SouthWestSensor Ltd, Enterprise House, Ocean Village, Southampton,SO14 3XB, United Kingdom.

Abstract

Microfluidic-based chemical sensors take laboratory analytical protocols and miniaturise them into field-deployable systems for *in situ* monitoring of water chemistry. Here we present a prototype nitrate/nitrite sensor based on droplet microfluidics that in contrast to standard (continuous phase) microfluidic sensors, treats water samples as discrete droplets contained within a flow of oil. The new sensor device can quantify the concentrations of nitrate and nitrite within each droplet and provides high measurement frequency and low fluid consumption. Reagent consumption is at a rate of 2.8 ml/day when measuring every ten seconds, orders of magnitude more efficient than the current state of the art. The sensor's capabilities were demonstrated during a three-week deployment in a tidal river. The accurate and high frequency data (6 % error relative to spot samples, measuring at 0.1 Hz) elucidated the influence of tidal variation, rain events, diurnal effects, and anthropogenic input on concentrations at the deployment site. This droplet microfluidic-based sensor is suitable for a wide range of applications such as monitoring of rivers, lakes, coastal waters, and industrial effluents.

Introduction

Monitoring nutrient levels in natural waters (oceans, lakes and rivers) is important for understanding the underlying biogeochemical processes and safeguarding against the effects of anthropogenic pollution. Traditionally, nutrients and other chemical parameters are measured by taking samples, either manually or *via* autosamplers,[1] then transporting the samples to a laboratory for later analysis. Using sensors to monitor *in situ* offers an attractive alternative, with the removal of sample transport allowing greater numbers of measurements and eliminating the risk of sample deterioration in transit.[2] Furthermore, pollution events can be detected in real time, allowing early warning and quicker, more effective remediation.

Nitrate and nitrite are key macronutrients in natural waters and are often implicated in anthropogenic nutrient pollution that leads to algal blooms and eutrophication.[3] Field deployable sensors have been developed to monitor nitrate and nitrite levels, both in academia and commercially.[4] The most widely used sensors are based on *in situ* UV spectrophotometry.[5] While marketed as "nitrate" sensors, the overlap of the nitrate and nitrite absorbance spectra mean that the sensors in fact measure combined nitrate and nitrite (ΣNO_x^-). The UV sensors can measure at high frequencies (a maximum of ~1 Hz) meaning that the sensors can be used on fast-moving platforms (e.g profiling floats,[7] surface vehicles[8]) to spatially map ΣNO_x^- concentrations. The high frequency measurement is also important for capturing and characterising episodic events. For example in rivers, where nutrient export can be dominated by storm events,[9, 10] high resolution monitoring is essential for deriving accurate estimates of nutrient loading[9] and differentiating input mechanisms.[11]

An alternative way to monitor nitrate and nitrite is by using wet chemical sensors. These sensors operate on similar principles to laboratory auto-analysers: pulling a water sample in, performing a chemical assay, and then recording or relaying the result using on-board electronics.[12,13, 14] By careful engineering of fluidic manifolds and control systems the whole system can be miniaturised

into a small integrated field-deployable package ("sensor"), with commercial systems available (e.g. Systea WIZ,[15] Seabird Scientific HydroCycle-PO_4[16, 17]). Recent academic developments of wet chemical sensors have focussed on reducing channel dimensions to a few hundred microns or less ("microfluidic sensors"), to improve fluid and power efficiency by reducing the fluidic volume and hence the required liquid volume and pumping.[2] Relative to *in situ* spectrophotometry, microfluidic sensors offer lower limits of detection (e.g. 25 nM[12] *versus* 2.4 µM[6]) and lower power requirements (e.g. 1.5 W[12] *versus* 7-8 W for commercial systems[6, 18]). Moreover, while UV spectrophotometry is restricted to a few chemical species (ΣNO_x^-, bromide and bisulfide)[5] microfluidic sensors can be adapted to monitor a wide range of chemical parameters including macronutrients (ΣNO_x^-, nitrite, phosphate, ammonia),[12, 19-24] micronutrients (e.g. Mn, Fe),[25-27] and carbonate system parameters.[28] Nonetheless microfluidic sensors face several challenges before they can become widespread. Microfluidic sensors measurement rates are slow (a maximum of every few minutes)[2] and fluidic architectures are also typically complex, requiring bespoke microfabricated manifolds and multiple separate valves and pumps.[12, 21, 23, 27] The added complexity increases possible failure modes and moreover increases the material cost of the sensor. However it is the use of consumable fluids (reagent, standards, blanks) which is the key limiting factor. Fluids must be periodically replaced, which increases running costs and discourages remote deployments, the size of the overall sensor unit is increased and the number of measurements that can be performed is fundamentally limited.

In this report we present a new type of microfluidic sensor based on a droplet flow regime. Relative to existing microfluidic systems our droplet-based sensor consumes orders-of-magnitude less reagent per measurement, can provide high frequency measurement, and requires fewer fluidic actuators (pumps and valves). In droplet flow, the aqueous sample is carried as a sequence of discrete droplets within a flow of immiscible oil[29] which do not contact the channel walls. Chaotic advection within droplets enhances mixing whereas in continuous microfluidics[30] laminar flow leads to slow diffusion-limited mixing which inherently limits measurement frequency. In continuous (non-droplet) microfluidics, viscous drag at the channel walls effectively smears the

composition of the sample as it travels downstream (referred to as Taylor dispersion),[30, 31] but in droplet flow droplet composition is maintained.[32] This allows the same droplet to be measured at different reaction times,[33] means the fidelity of time-dependent chemical signals is better preserved within the system,[34] and channel flushing between samples is no longer needed, reducing the amount of fluid used in flushing and power expended in pumping.

Currently droplet microfluidics is restricted to the laboratory, used for a variety of biochemical and chemical applications such as digital PCR, single cell analysis, and high throughput screening.[35-41] For those applications droplet microfluidics typically requires expensive bulky equipment, such as high precision pumps and complex optical systems, but despite this droplet generation is still easily perturbed (e.g. by changes in ambient conditions, fluidic pressure changes, air bubbles, and impurities in liquids). We recently developed a method for robust droplet generation that is insensitive to perturbations.[42] The droplet generation is driven by small, affordable pump technology, and hence is well-suited for field-deployable systems.[43] Using this approach, nitrate measurement in droplets was first demonstrated in a laboratory setting, with alternating droplets of sample and a standard allowing realtime calibration of the sample measurements.[44] There it was found that decomposition of nitrite under acidic conditions generated nitrate and nitric oxide, with the latter diffusing between droplets and resulting in inter-droplet crosstalk. Here, we address that nitrate/nitrite-specific crosstalk problem by modifying the microfluidic design to allow either sample or standard flow at any given time and hence remove crosstalk. Moreover, the system has been fully developed into a field-deployable sensor device for monitoring natural waters which, additionally, can monitor both nitrate and nitrite concentrations simultaneously.

The sensor prototype was first characterised in the laboratory and then demonstrated in a three week deployment in a tidal river, where tide, rain events, diurnal, and anthropogenic effects were all seen to contribute to fluctuations in environmental nitrate/nitrite levels. When monitoring at a rate of a measurement every 10 seconds (8640 measurements/day), reagent consumption is only

2.8 ml/day, meaning one litre of reagent would be sufficient for approximately 11 months of continuous operation.

Experimental

The sensor operates as illustrated in Fig. 1a. Water is drawn into the sensor by a peristaltic pump built in-house[42, 44] (common to all fluidic lines), passing first through a valve which can swap the sample for an on-board standard at user-specified intervals to allow for *in situ* calibration. The water sample then travels through the pump and into a fluidic junction where it meets a reagent flowing at the same volumetric flow rate. Here a 1:1 sample:reagent ratio is used to ensure balanced flow rates and fluidic backpressures. In the future the ratio could be increased by either changing the pump line internal diameters or the mechanical design of the peristaltic pump,[42] which could decrease sample dilution and hence increase sensitivity. After the sample and reagent flows have met, they are then immediately broken into a stream of droplets by introduction of a fluorinated oil (Fluorinert FC40) at a T-junction. The volumetric flow rate of oil is equal to the sum of the aqueous streams. Under standard flow rates (defined later) a single droplet is generated approximately every ten seconds. The droplet contents mix as they are carried downstream through PTFE tubing and the reagent reacts with the analyte to produce a coloured product (Fig. 1b). The assay used here is a variant on the traditional Griess method, whereby nitrate is first reduced to nitrite which then reacts with a mixture of sulfanilamide and N-naphthyl-ethylenediamine (NEDD) to produce a purple/pink coloured diazonium product.[1] In previously reported systems, the reduction step was achieved by flowing the sample over a solid copper-treated cadmium surface.[12, 20, 23] While highly effective in continuous microfluidics, this method is not appropriate for droplet flow as a layer of oil always separates the droplet contents from the solid channel walls. Here instead vanadium chloride (VCl_3) is added to the standard Griess reagent to act as reducing agent[45-48] (loading 0.5 wt%, see ESI).

The strength of the colour is quantified downstream by absorption flow cells comprising simple optical components (LEDs, light to voltage converters) within a micromilled structure[49] (example raw data is shown in Fig. 1c). Each droplet constitutes a single discrete measurement point. Droplet absorbance is calculated using a modified version of the Beer-Lambert law[33, 50] which accounts for the light transmitted through the transparent neighbouring oil segments (see ESI). In this way the oil operates as a quasi-blank which will correct for any perturbations to light source intensity or light path. Consequently, while a blank measurement must be performed before or after each deployment to benchmark the oil levels (by flowing pure water through the inlet), the sensor does not require an on-board blank.

An inline heater comprised of PTFE tubing surrounding a resistive heater is included to accelerate the reaction. The heater is measured by an internal thermistor and controlled by an proportional–integral–derivative (PID) algorithm and custom electronics (not shown in Fig. 1a) so that a constant temperature is maintained with an error less than 0.1°C. This ensures the reaction within the droplets occurs at a reproducible temperature irrespective of ambient conditions. The electronics were designed in-house and also control the pump and relay the flow cell data. All droplets and oil are finally collected in a waste bag, where the dense fluorinated oil gravimetrically separates from the aqueous waste to be reused. All fluidic conduits in the sensor were composed of off-the-shelf tubing for ease of fabrication. All components are packaged into a water-tight cylinder (Fig. 1d, diameter 102 mm, length 226 mm) with the exception of power, supplied *via* a 5 V USB (universal serial bus) cable, and the fluid reservoirs (oil, reagent, and standard) which are contained in an external housing and coupled *via* a penetrator connection. All fluids are packaged in light- and air-impermeable laminated plastic/aluminium foil bags as the dissolved vanadium(III) within the reagent is easily oxidised when exposed to ambient conditions. Stored in this way we found that reagent still performed at an equivalent level to fresh reagent after 9-months' storage at room temperature (data not shown).

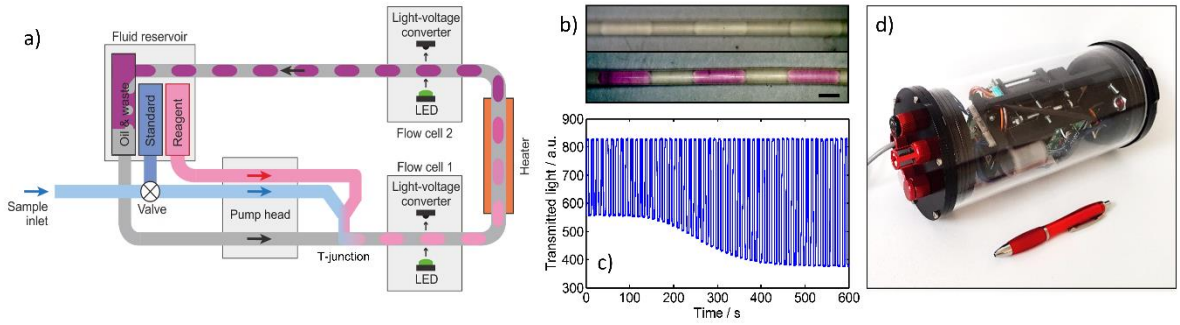

Figure 1: a) Schematic showing the fluidics of the sensor and illustrating the mode of operation. b) Droplets of reagent and 200 µM nitrate within PTFE tubing (0.5 mm inner diameter, 0.7 mm outer diameter). The droplets are shown immediately before (top) and after (bottom) travelling through the heater (50 °C, 7.2 mins residence time). A 1 mm scale bar is shown bottom right. c) Example raw data from a flow cell taken over ten minutes, during which 54 droplets (low light transmission) and oil segments (high light transmission) pass through the light path producing a characteristic square wave profile.[33, 49] d) Image of a finished sensor incorporating fluidics, heater, flow cells and control electronics. The external fluid reservoir is not shown. A pen is shown for scale.

The use of a peristaltic pump here rather than solenoid[20] or syringe pumps,[12, 21] means that a single unit can drive all fluid lines with only one valve required - reducing complexity and cost. Importantly, the use of peristalsis as a pumping method ensures robust droplet generation *via* our previously reported anti-phase peristaltic approach.[42] This takes advantage of the pulsatile nature of peristaltic pumping, alternately injecting the aqueous and oil phases into the T-junction such that each oil pulse "chops off" the preceding aqueous pulse into a discrete droplet. As described elsewhere,[42] the pump can be rationally designed to deliver droplets with pre-defined volumes and numbers per turn of the motor shaft. Importantly, this method delivers highly reliable and robust droplet generation that is independent of flow rate and liquid properties, making it highly desirable for a field deployable sensor device.[42]

Additional details of sensor fabrication and reagent formulation are included in the ESI.

Results and Discussion

Nitrate reduction

Vanadium(III)-mediated reduction is much slower than the previously-reported method of heterogeneous reduction by cadmium, with reaction times of several hours at room temperature.[45-47] To accelerate the reaction and reduce the reaction time to minutes, an inline heater was included in the sensor design (Fig. 1a). The reduction rate is controlled by both temperature and reaction time, hence we systematically varied the heater temperature and the residence time of the droplets to find the optimum reaction conditions, as shown in Fig. 2. At 40 °C, the absorbance increased with residence time but did not peak despite times of up to 25 minutes. Conversely at higher temperatures the absorbance peaked but then decreased at longer residence times - an effect which has previously been attributed to the degradation of the diazonium product by vanadium(III).[45-47] Selecting the optimum conditions involves balancing operational requirements with analytical performance. We chose 50 °C and 7.1 minutes (a total flow rate of 11.0 µL/min) as optimum because while higher temperatures and shorter reaction times produced higher absorption (e.g. 60 °C and 4.9 mins gives 7 % higher absorbance), the chosen conditions offered improved operational conditions: The lower temperature reduces power consumption, while the residence time of 7.1 minutes sits on a plateau (Fig. 2) meaning changes in residence time (± 2 mins) could be tolerated without affecting colour development. Operating under these conditions the sensor device consumes a power of 1.5 W, with the pump, heater and control electronics each consuming approximately 0.5 W. The total power consumption is equivalent to the current state-of-the-art (continuous flow) microfluidic sensors,[12, 21] and approximately five times lower than modern commercially-available nitrate sensors based on *in situ* ultraviolet spectrophotometry.[6, 7, 18]

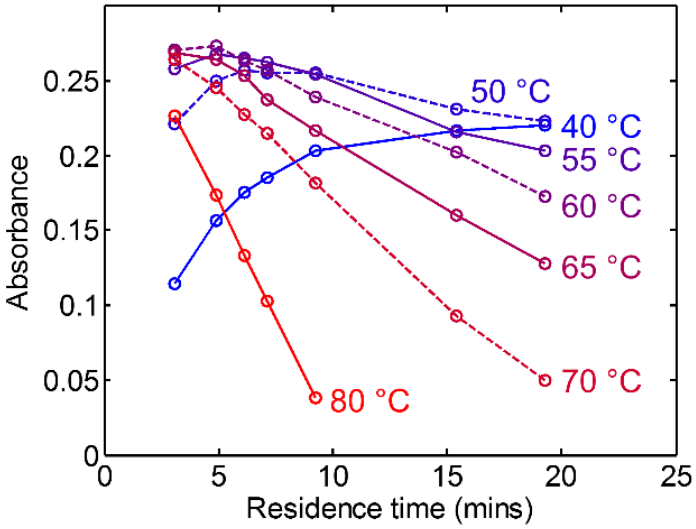

Figure 2: The absorbance of droplets containing 500 µM nitrate and reagent subjected to different temperatures and residence times within the heater.

The very different speeds of the two nitrate reaction steps (reduction by vanadium(III), then Griess reaction) can be harnessed in the sensor design to measure both nitrite and ΣNO_x^-. As the standard Griess reaction occurs much faster than the reduction step (<60 s at room temperature) it should be possible to first quantify nitrite in the sample under ambient temperature, and then heat the droplets to drive the nitrate reduction and quantify the ΣNO_x^-. To achieve this we positioned absorbance flow cells immediately before (flow cell 1, Fig. 1a) and after the heater (flow cell 2, Fig. 1a). If required the nitrite concentration can then be subtracted from the ΣNO_x^- to obtain the nitrate concentration alone. This ability to be able to quantify both nitrite and nitrate in the same sample is unique in microfluidic sensors where systems can typically either measure nitrite or ΣNO_x^-.[14, 20, 23, 24, 51, 52]

Concentration response

To characterise the sensor's analytical performance, we pumped nitrate and nitrite standards through the device at the chosen heater temperature and flow rate. Fig. 3 shows the response observed by flow cell 1 (before heating, Fig. 3a) and flow cell 2 (after heating, Fig. 3b) for different

concentrations of nitrate (red squares) and nitrite (blue circles). As expected, flow cell 1 (before heating) gave a strong response for nitrite, with a linear relation that passed through the origin. Under the ambient conditions of the laboratory (~21 °C), nitrate produced a slight response (line of best fit 32 M^{-1} *versus* 841 M^{-1} for nitrite), indicating that a small quantity of nitrate had been reduced to nitrite in the 2.3 minutes it took the droplets to reach flow cell 1. By contrast, flow cell 2 (after heating, Fig. 3b) gave a strong response for both nitrite and nitrate, consistent with the heater having successfully accelerated the nitrate reduction. The nitrate response was reproducibly lower than the nitrite response (line of best fit 682 M^{-1} *versus* 839 M^{-1}) and is consistent with the previous observation that the chosen reaction conditions don't deliver maximum nitrate conversion (Fig. 2). The different contributions from nitrite and nitrate to the measured absorbance need to be taken into consideration when calculating ΣNO_x^- from flow cell 2 measurements. In aerated waters nitrite is typically two orders of magnitude less concentrated than nitrate[1, 53] and hence it is practical under these conditions to approximate nitrite as having the same sensitivity as nitrate. This assumption will result in a 0.3 % overestimation of ΣNO_x^- and as the error is small we used this approximation in the deployment described below (see supplementary experimental, ESI). In cases where nitrite concentrations are more significant (e.g. anoxic waters) this approximation would not be appropriate, however the signal from flow cell 1 could be used to account for nitrite contributions in flow cell 2. Overall, nitrate and nitrite both gave reproducible linear responses that allow quantification of both species up to at least 800 μM with the different responses allowing differentiation of the separate species.

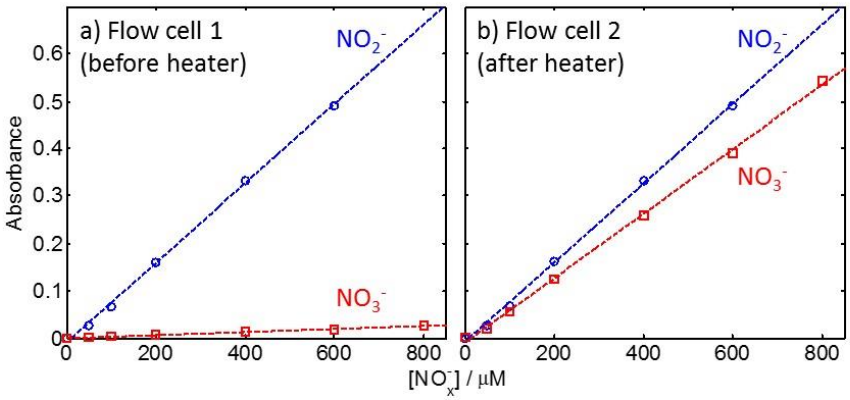

228

229 *Figure 3: Droplet absorbance with different concentrations of nitrite (blue circles) and nitrate (red*
230 *squares). In flow cell 1, positioned before the heater, (a) the fast reaction of nitrite generates a*
231 *strong linear response, with a much weaker one from the unreactive nitrate. In flow cell 2,*
232 *positioned after the heater, (b) strong linear responses are seen for both nitrate and nitrite.*

233 Changes in refractive index caused by changes in salinity can alter the light path through the flow
234 cell and hence lead to false readings. To counter this, an additional flow cell can be placed on the
235 inlet stream to monitor changes in refractive index.[12] We included this on earlier prototypes,
236 however we chose not to include it here to simplify the system and because initial field tests at our
237 test site (described later) did not find measurable refractive index changes due to the small range
238 in salinity.

239 The limit of detection (LOD) was determined to be 1.7 µM using the 3-sigma method[54] (see ESI) but
240 can be further reduced by taking advantage of the high temporal measurement frequency by
241 averaging data points (e.g. the limit of detection reduces to 0.7 µM when averaging +/- 3 mins, see
242 supplementary experimental, ESI). Relative to existing microfluidic systems where LODs have been
243 reported to 0.1 µM [23] or lower,[12] this LOD is high and results from the relatively short optical path
244 length of the flow cells (0.5 mm). Currently the flow cells illuminate the elongated droplets (Fig. 1b)
245 across their shorter axis.[33, 49] As sensitivity in absorption measurements is proportional to optical
246 path length[55] an approximate eight-fold improvement could be obtained by illuminating along the

long axis of the droplets,[56] with further gains possible by elongating the droplets within narrower channels.

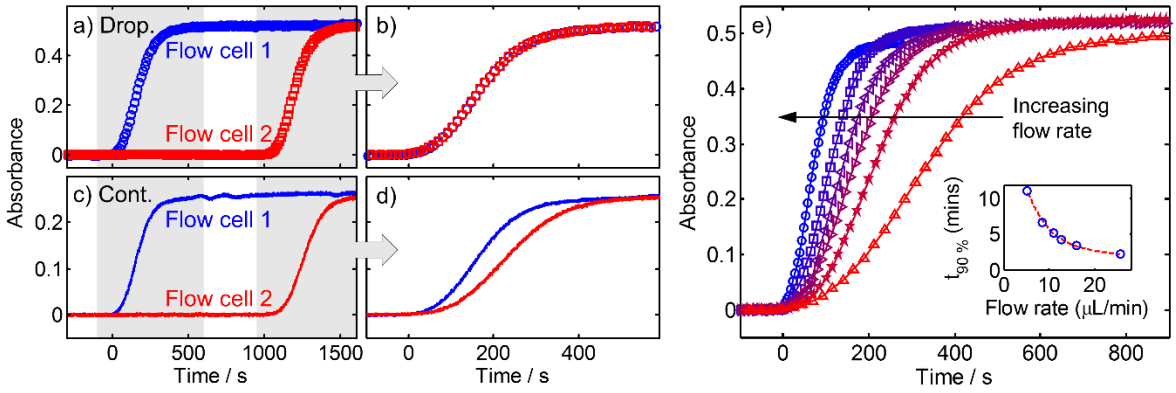

Figure 4: Time response of the sensor to step changes in nitrite concentrations (0 to 600 μM) at the sensor inlet. a) The responses of flow cell 1 (blue circles) and flow cell 2 (red squares) with the sensor under normal conditions. Each marker corresponds to the measurement of a single droplet. To compare the temporal response of each flow cell, the grey shaded areas are shown in (b) taking t=0 as the moment the signal began to change for each flow cell. The responses of each flow cell directly superimpose each other. c) The responses of flow cell 1 (blue trace) and flow cell 2 (red trace) with the sensor operating under continuous flow by replacing the oil with deionised water. When the responses of the two flow cells are compared (d), flow cell 2 has a noticeable time lag. e) Absorbance data from flow cell 1 with changing total flow rate. As the flow rate increases from 5.10 to 25.5 μL/min, the changeover becomes faster, with the time taken to reach 90 % of the final plateau value shown inset.

Temporal response versus *continuous flow*

In droplet flow, the chemical composition of the droplets is maintained as they travel downstream, unaffected by the Taylor dispersion that characterises continuous flow. To demonstrate this, and to also characterise how quickly the sensor responded to composition changes at the inlet we measured the response of the two flow cells to a step-change in concentration: from deionised water to 600 μM nitrite under standard flow conditions (11.0 μL/min total flow rate, a droplet

generated every 10 s). Fig. 4a shows the absorbance change observed by flow cell 1 (blue circles) and flow cell 2 (red squares), with each marker corresponding to a single droplet. In each case, the absorption increased from 0 to plateau at 0.52 over approximately 6 minutes (5.2 minutes to reach 90 % of maximum in each case), and with the droplets taking 17.2 minutes to travel from flow cell 1 to flow cell 2. When the response from each flow cell is adjusted such that the time offset between the two flow cells is removed (Fig. 4b) the response for each droplet directly overlays each other, showing how the composition of the droplets was exactly maintained through the system, with a fixed travel time between flow cell 1 and 2.

The changeover time of 6 minutes resulted from the Taylor dispersion within the segment of continuous flow from the inlet to the T-junction where droplets were generated. This was confirmed by running the same experiment under continuous flow conditions (Fig. 4c) where the total flow rate was maintained by replacing the oil with deionised water. Here an almost identical temporal response is observed in flow cell 1 (5.0 minutes to reach 90 % of maximum) as both experiments had a very similar fluidic architecture upstream of flow cell 1, only differing by the relatively small volume between droplet generation and flow cell 1. In contrast to droplet flow, in continuous flow the temporal response became worse as the fluid travelled through the sensor, with the transition taking 30 % longer at flow cell 2 (6.5 minutes to reach 90 % of maximum), causing signal broadening and making it difficult to correlate the data from the two flow cells (Fig. 4d). Thus the use of droplet flow not only gives the optimum temporal response in flow cell 2, but moreover allows simple correlation of the data from each flow cell- enabling easy quantification of both nitrite and ΣNO_x^- for the same sample volume.

For most applications 6 minute resolution is more than adequate, however increased temporal resolution (e.g. for water column profiling[40]) can be achieved by reducing the fluidic volume between the inlet and droplet generation or by increasing the total flow rate. Fig. 4e shows transitions for flow rates from 5.10 to 25.5 µL/min, with the times required to reach 90 % of

maximum shown inset. Increasing flow rate decreases transition time to as low as 2.2 minutes to reach 90 % at a total flow rate of 25.5 µL/min. Increasing the flow rate will increase fluid and power usage, however in scenarios where higher temporal resolution is required it is unlikely to be needed for extended periods.

Deployment in tidal river

Having characterised the sensor in the laboratory we used it to continuously monitor the variation of ΣNO_x^- and nitrite concentrations in a tidal river. The River Itchen is a chalk river on the south coast of the UK, which feeds into the Southampton Water estuary and ultimately into the English Channel. The sensor was deployed from mid-July 2018 following a prolonged dry period, with no rainfall in the local area for approximately 6 weeks.[57] The deployment location (illustrated in Fig. S1) was ~250 m downstream of the Woodmill tidal barrier at a location (50°56'02.1"N 1°22'48.0"W) subject to several metres tidal variation. The sensor was suspended from a pontoon (shown in supplementary Fig. S2) with the water sample intake a constant ~50 cm under the surface throughout the deployment. A logging conductivity and temperature sensor (WTW, LF340 measuring every 15-30 mins) was deployed alongside the sensor, and grab samples were taken twice daily during weekdays for lab analysis (see supplementary experimental, ESI). The sensor was operated continuously, generating a droplet (a single measurement) every 10 s, and the onboard standard (200 µM nitrite) was flowed through the system for a period of 30 minutes every 6 hours. A blank of deionised water was run through the inlet in order to benchmark the oil quasi-blank measurements immediately before deployment.

Over the course of the deployment the measurements of the on-board standard remained approximately constant, with relative standard deviations of 5.3 % and 4.9 % relative to the long term mean for flow cell 1 and flow cell 2 respectively (Fig. S3). The absorbance of the river water (sample) droplets was much higher in flow cell 2 (after heating) than flow cell 1 (before heating, see Fig. S3) indicating a predominance of nitrate over nitrite, as expected for aerated waters.[53] The

sample absorbance fluctuated over time in both flow cells, indicating highly variable nitrate and nitrite concentrations in the river.

Fig. 5a shows the variations in the ΣNO_x^- concentration derived from flow cell 2 (light blue dots, and blue line rolling average), along with results from the grab samples (red circles and error bars). The ΣNO_x^- values are in the previously reported range for the river,[12, 58-60] and the sensor data is in good agreement with the grab sample results, differing by a mean relative error of 6.4 %. For comparison, the ΣNO_x^- data is plotted alongside conductivity (Fig. 5b), tide height measured downstream at Southampton docks[61] (Fig. 5c), and local rainfall in Southampton[57] (Fig. 5d). The variation of temperature, river discharge, and barometric pressure are also shown in supplementary Fig. S4.

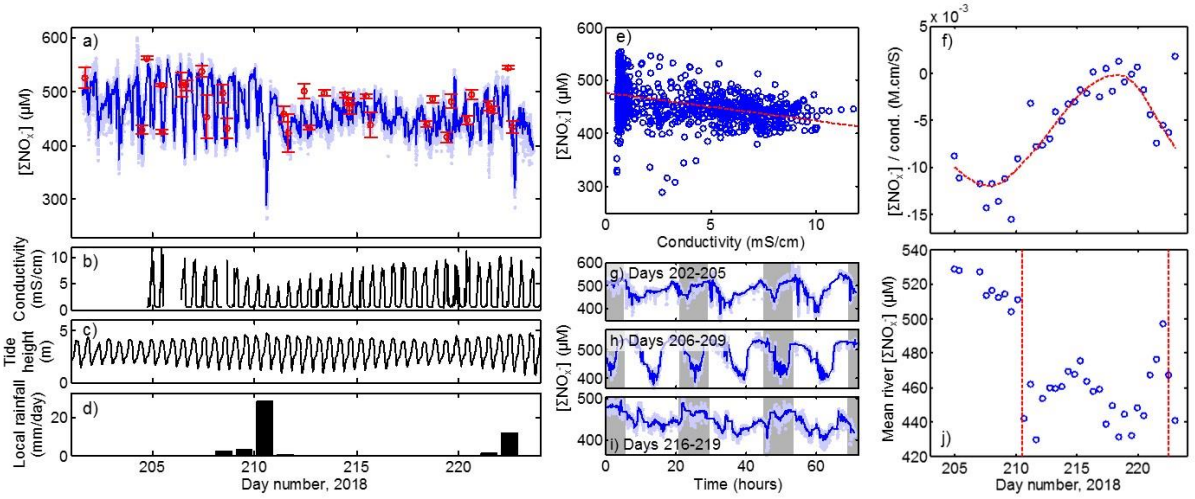

Figure 5: a) ΣNO_x^- values derived from flow cell 2 (after heating). Each light blue point corresponds to a measurement of a single droplet, while the dark blue line is a rolling average (median value ± 3 minutes, reflecting the changeover time). The red markers correspond to concentrations obtained from lab-analysed grab samples, with error bars corresponding to the standard deviation of replicate measurements. b) Conductivity of the river at the deployment location. c) Tide height measured downstream at Southampton docks.[61] d) Rainfall measured in Southampton.[57] e) The relation between ΣNO_x^- and conductivity, shown with a line of best fit indicating the overall negative

correlation. f) Plot showing how the gradient of the line of best fit of the ΣNO_x^-/conductivity relation, illustrated in (e), varied during the deployment. Each data point corresponds to the correlation during a tidal cycle (low tide to low tide), while the red dashed line shows a guide to the eye. g) The ΣNO_x^- variation during the 72 hours between days 202 and 205, shown alongside the variation during days 206 to 209 (h) and days 216 to 219 (i). Night is indicated by the grey shaded regions. j) Plot showing the mean ΣNO_x^- of the incoming freshwater stream during each tidal cycle. The timing of major rain events (d) are shown as vertical red dashed lines.

The data indicates that ΣNO_x^- concentration during the deployment was affected by a combination of tidal cycles, rain input, and diurnal effects. The tidal effect was most obvious between days 204 and 210 where the ΣNO_x^- fluctuated by up to 28 % of peak value in each cycle (day 207). Peaks coincided with low tide when nutrient-rich fresh water predominated and then dropped with the inflow of nutrient-poor seawater at high tide. As might be expected, the conductivity measurements varied in opposition, typically 0.65 mS/cm at low tide then rising to between 4 and 10 mS/cm at high tide, with the peak conductivity dependent on the magnitude of the tide (see Fig. 5b,c).

To examine the influence of tidal effects on ΣNO_x^- concentrations in more detail we considered the relationship between ΣNO_x^- and conductivity (a proxy for seawater content). As shown in Fig. 5e, overall there was an expected negative correlation (higher seawater content increasing conductivity and lowering nutrient concentrations), however the magnitude of the ΣNO_X^- /conductivity correlation varied over the course of the deployment, as shown in Fig. 5f. The correlation (derived from the gradient of a line-of-best-fit for each tide) smoothly shifted from its most pronounced value of -0.01 M.cm/S around day 208, to zero between days 216 and 220 (i.e. tide has minimal effect on ΣNO_x^-) and again grew towards the end of the deployment. The peak/nadir of the correlation roughly coincided with the neap/spring tides respectively (Fig. 5c), however a longer deployment would be needed to confirm this and investigate further.

When the tidal influence was at its lowest, the ΣNO_x^- showed evidence of diurnal variation. Fig. 5g-i compares the ΣNO_X^- variation during three periods of different tidal influence: low during days 202-205 (Fig. 5g), high during days 206-209 (Fig. 5h), and again low during days 216-219 (Fig. 5i). In each case 72 hours' data is shown, with night times indicated by grey shaded regions. During the periods of low tidal variation (Fig. 5g,i), peaks corresponding to tidal effects are superimposed on a predominant 24 hour cycle (most notably in Fig. 5i) with ΣNO_x^- lower during the day and peaking during the night . This effect is less obvious during the periods of high tidal variation as it is masked by the much larger tidal changes, but it is still perceivable. In Fig. 5h for example, the high tides coincide with the middle of the night and day. If we look at the corresponding ΣNO_x^- troughs, each of the daytime minima are lower than their neighbouring night time minima by approximately 20 μM. This is unlikely to be a measurement artefact from ambient temperature variation as the heater provided a constant, defined temperature for nitrate reduction. Diurnal cycles in rivers can be due to the daily variation of sewage treatment works (STW) discharges.[62] The discharge from the nearest STW (Portswood STW, Fig. S1) has been previously found to lower nitrate levels,[59] however as it was downstream of the deployment location we would expect contributions from this STW to occur on a timescale determined by the tidal cycle. The nearest upstream STW is at Eastleigh, approximately 5 km away, but a previous study found it did not affect river nitrate levels.[59] The diurnal variation could be due to primary production in the river, with the removal of ΣNO_x^- coinciding with the daylight required for photosynthesis, however additional measurements (e.g. dissolved oxygen) would be needed to definitively confirm this hypothesis.

Rain events also had a noticeable effect on ΣNO_x^- levels. There were two significant rain events on day 210 and 222 (Fig. 5d) which immediately resulted in sharp transitory dilutions (<12 hrs) of the ΣNO_x^- concentration by 42 % and 24 % respectively (Fig. 5a). It was followed by less pronounced but more prolonged dilution of the river water input. This is shown in Fig. 5j which shows the river ΣNO_x^- concentrations over time. The values used here constitute the river concentration independent from tidal effects by taking the mean values at low tide (defined as conductivity

386 <0.7 mS/cm). The timing of each rain event is marked on Fig. 5j as a red dashed line and coincide
387 with sharp and prolonged drops in river ΣNO_x^-.

388 Fig. 6a shows the variations in the nitrite concentration derived from flow cell 1 (light blue dots,
389 and blue line rolling average). Nitrite concentrations in the River Itchen are typically single-figure
390 values,[58-60] hence the observed concentrations (up to almost 50 µM) included concentrations
391 approximately ten times higher than expected. In trying to explain this, our attention initially
392 turned to the sensor. As previously noted, there could be a small increase in absorbance due to the
393 reaction of a proportion of nitrate prior to heating (as shown in Fig. 3a). In a worse-case scenario
394 (ambient temperatures routinely > 20 °C) this would have artificially raised the nitrite reading by a
395 maximum of 5 µM and hence was too small to account for the observed concentrations (as an
396 aside we note that this contribution could be quantified and corrected in future by using a nitrate
397 standard in place of the nitrite standard used on this deployment). Additionally, the theory that
398 nitrate reaction was responsible for the unexpected nitrite measurements was inconsistent with
399 the observed fluctuations in nitrate-dominated ΣNO_x^- and nitrite. Whereas ΣNO_x^- fluctuated daily
400 by up to 28 % (day 207), nitrite levels varied by up to 90 % (day 223). Moreover, whereas the ΣNO_x^-
401 variation showed a negative correlation with conductivity (Fig. 5e), the nitrite showed the exact
402 opposite trend, with a universally positive correlation (Fig.6b, more detail shown in supplementary
403 Fig. S5) - indicative of differing major sources for nitrate and nitrite at the deployment site. As such
404 we determined the high nitrite measurements were not sensor artefact.

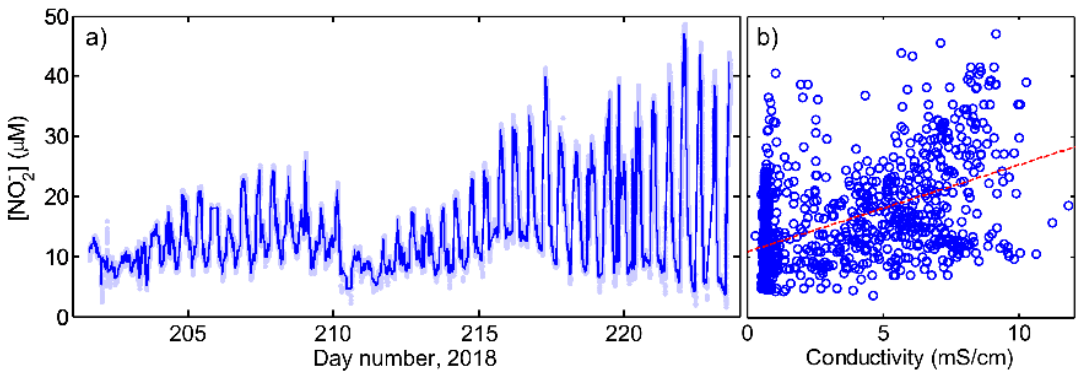

405

Figure 6: a) Nitrite values derived from flow cell 1 (before heating). Each light blue point corresponds to a measurement of a single droplet, while the dark blue line is a rolling average (median value ± 3 minutes, chosen to reflect the changeover time). b) The relation between nitrite and conductivity values, shown with a line of best fit which indicates the overall positive correlation.

The source of the elevated nitrite measurements became evident when considering the deployment location, which was approximately 400 m upstream of Portswood STW (Fig. S1). It has been generally noted that STW outputs contribute to increased river nitrite concentrations[53] and a previous study quantifying nutrient levels along the length of the Itchen found locally elevated nitrite concentrations (up to 44 µM) near the outflow of the same STW.[59] Hence it is likely that the high nitrite concentrations and the positive nitrite/conductivity correlation resulted from effluent being carried upstream from the STW on each incoming tide. As we do not know the discharge volumes, compositions, or timings from the STW it is difficult to read too much into the nitrite data, however speculation on the trends in nitrite/conductivity correlation is given in the supplementary information (Fig. S5 and accompanying text). It is noticeable that the rain event on day 211 (Fig. 5d) coincided with a decrease in nitrite peak magnitude that lasted several days (Fig. 6a). This could be due to the accompanying increase in river discharge (supplementary Fig. S4) providing increased hydrodynamic resistance to the incoming tide and thus reducing the amount of STW effluent carried upstream.

During the three week deployment over 160,000 river samples were measured for nitrate and nitrite. The high measurement rate (0.1 Hz) is notably faster than previous microfluidic sensors based on continuous (non-droplet) microfluidics, where measurement times are typically a minimum of several minutes.[12-14, 21, 23, 27] This high frequency is advantageous as it makes finer structure in concentration variation visible, allows for averaging to reduce instrumental noise and hence reduce limits of detection. It also indicates that the sensor can be used on profiling platforms or moving vehicles.[40]

Despite the high measurement frequency, the low total flow rate within the sensor meant the fluid consumption of the sensor was markedly lower than previously reported systems. Low fluid consumption is important as this, along with power considerations, determines the length and/or measurement frequency of a sensor deployment. Reagent was consumed at a rate of 2.8 ml/day, while the combined consumption for sample and standard was also 2.8 ml/day. The oil was continuously recycled and hence not consumed. This corresponds to a consumption of 350 nL of reagent for each measurement – three orders of magnitude lower than the best previously reported microfluidic nitrate sensors.[12, 23] However as previously reported systems have included sample changeover in their fluid economy calculations, a fairer comparison might be to also include the 6 minute changeover time when calculating the consumption for our sensor. Even allowing for the changeover, it corresponds to 12 µL of reagent usage, still 30 times lower than current state-of-the-art systems.[12] It should be emphasised that the reagent consumption of 2.8 ml/day means that 1 L of reagent would last over 11 months whilst still continuously measuring at a rate of once every 10 seconds.

In this instance, the sensor generated a continuous stream of droplets performing a single reaction, however in the future droplet flow could be used for multiplexed analysis. As each droplet is a self-contained chemical reaction vessel, it is possible to generate sequences of droplets of arbitrarily defined composition. This could be used, for example, to generate droplets of alternating sample and standard,[44] or series of droplets to sequentially assay different analytes. In principle most analytes that can be measured using a colorimetric assay, such as the modified Griess assay used here, could be measured using this system. The absorption flow cells could also be swapped for fluorescent or chemiluminescent equivalents to further expand the available assay options.

Supporting Information

Supplementary experimental describing sensor fabrication, reagent formulation, data processing, and spot-sampling methods in closer detail. Supplementary results include additional discussion of deployment nitrite results.

Author Information

Corresponding Author

*E-mail: x.niu@soton.ac.uk

Acknowledgements

This work was supported by funding from the Natural Environment Research Council UK (NE/P004016/1, NE/S013458/1) and the Engineering and Physical Sciences Research Council UK (EP/M012425/1). AMN is supported by an Industrial Innovation Fellowship from the Natural Environment Research Council (NE/R013578/1). We thank the Environment Agency for river discharge data provided under the Open Government Licence v3.0, Chris Tuffill and Keith MacFadyen for their help setting up the sensor deployment, and Alex Beaton of the National Oceanography Centre for initially suggesting the vanadium-based Griess assay.

References:

1. Grasshoff, K.; Kremling, K.; Ehrhardt, M., *Methods of Seawater Analysis*. 3 ed.; Wiley-VCH: 1999.
2. Nightingale, A. M.; Beaton, A. D.; Mowlem, M. C., Trends in microfluidic systems for in situ chemical analysis of natural waters. *Sensors and Actuators B: Chemical* **2015,** *221* (Supplement C), 1398-1405.
3. Burt, T. P.; Howden, N. J. K.; Worrall, F.; Whelan, M. J., Long-term monitoring of river water nitrate: how much data do we need? *Journal of Environmental Monitoring* **2010,** *12* (1), 71-79.
4. Bende-Michl, U.; Hairsine, P. B., A systematic approach to choosing an automated nutrient analyser for river monitoring. *Journal of Environmental Monitoring* **2010,** *12* (1), 127-134.
5. Johnson, K. S.; Coletti, L. J., In situ ultraviolet spectrophotometry for high resolution and long-term monitoring of nitrate, bromide and bisulfide in the ocean. *Deep Sea Research Part I: Oceanographic Research Papers* **2002,** *49* (7), 1291-1305.
6. Sea-Bird Scientific SUNA V2 User Manual. **2018,** (SUNA180725).
7. Johnson, K. S.; Coletti, L. J.; Jannasch, H. W.; Sakamoto, C. M.; Swift, D. D.; Riser, S. C., Long-Term Nitrate Measurements in the Ocean Using the in situ Ultraviolet Spectrophotometer: Sensor Integration into the APEX Profiling Float. *Journal of Atmospheric and Oceanic Technology* **2013,** *30* (8), 1854-1866.
8. Hensley, R. T.; Cohen, M. J.; Korhnak, L. V., Inferring nitrogen removal in large rivers from high-resolution longitudinal profiling. *Limnology and Oceanography* **2014,** *59* (4), 1152-1170.
9. Bieroza, M. Z.; Heathwaite, A. L.; Mullinger, N. J.; Keenan, P. O., Understanding nutrient biogeochemistry in agricultural catchments: the challenge of appropriate monitoring frequencies. *Environ. Sci.-Process Impacts* **2014,** *16* (7), 1676-1691.
10. Cassidy, R.; Jordan, P., Limitations of instantaneous water quality sampling in surface-water catchments: Comparison with near-continuous phosphorus time-series data. *J. Hydrol.* **2011,** *405* (1-2), 182-193.
11. Bowes, M. J.; Jarvie, H. P.; Halliday, S. J.; Skeffington, R. A.; Wade, A. J.; Loewenthal, M.; Gozzard, E.; Newman, J. R.; Palmer-Felgate, E. J., Characterising phosphorus and nitrate inputs to a rural river using high-frequency concentration-flow relationships. *Science of the Total Environment* **2015,** *511*, 608-620.
12. Beaton, A. D.; Cardwell, C. L.; Thomas, R. S.; Sieben, V. J.; Legiret, F. E.; Waugh, E. M.; Statham, P. J.; Mowlem, M. C.; Morgan, H., Lab-on-Chip Measurement of Nitrate and Nitrite for In Situ Analysis of Natural Waters. *Environmental Science & Technology* **2012,** *46* (17), 9548-9556.
13. Grand, M. M.; Clinton-Bailey, G. S.; Beaton, A. D.; Schaap, A. M.; Johengen, T. H.; Tamburri, M. N.; Connelly, D. P.; Mowlem, M. C.; Achterberg, E. P., A Lab-On-Chip Phosphate Analyzer for Long-term In Situ Monitoring at Fixed Observatories: Optimization and Performance Evaluation in Estuarine and Oligotrophic Coastal Waters. *Frontiers in Marine Science* **2017,** *4* (255).
14. Beaton, A. D.; Wadham, J. L.; Hawkings, J.; Bagshaw, E. A.; Lamarche-Gagnon, G.; Mowlem, M. C.; Tranter, M., High-Resolution in Situ Measurement of Nitrate in Runoff from the Greenland Ice Sheet. *Environmental Science & Technology* **2017,** *51* (21), 12518-12527.
15. Wild-Allen, K.; Rayner, M., Continuous nutrient observations capture fine-scale estuarine variability simulated by a 3D biogeochemical model. *Marine Chemistry* **2014,** *167*, 135-149.
16. Gilbert, M.; Needoba, J.; Koch, C.; Barnard, A.; Baptista, A., Nutrient Loading and Transformations in the Columbia River Estuary Determined by High-Resolution In Situ Sensors. *Estuaries and Coasts* **2013,** *36* (4), 708-727.
17. Twardowski, M. S.; Townsend, D. W.; Sullivan, J. M.; Koch, C.; Pettigrew, N. R.; O'Donnell, J.; Stymiest, C.; Salisbury, J.; Moore, T.; Young-Morse, R.; Stockley, N. D.; Morrison, J. R., Developing the First Operational Nutrient Observatory for Ecosystem, Climate, and Hazard Monitoring for NERACOOS. *Marine Technology Society Journal* **2015,** *49* (3), 72-80.
18. OTT ecoN Operating Instructions. **2018,** (63.300.001.B.E. 01-0918).

19. Bey, S.; Connelly, D. P.; Legiret, F. E.; Harris, A. J. K.; Mowlem, M. C., A high-resolution analyser for the measurement of ammonium in oligotrophic seawater. *Ocean Dyn.* **2011,** *61* (10), 1555-1565.
20. Chapin, T. P.; Caffrey, J. M.; Jannasch, H. W.; Coletti, L. J.; Haskins, J. C.; Johnson, K. S., Nitrate sources and sinks in Elkhorn Slough, California: Results from long-term continuous in situ nitrate analyzers. *Estuaries* **2004,** *27* (5), 882-894.
21. Clinton-Bailey, G. S.; Grand, M. M.; Beaton, A. D.; Nightingale, A. M.; Owsianka, D. R.; Slavikt, G. J.; Connelly, D. P.; Cardwell, C. L.; Mowlem, M. C., A Lab-on-Chip Analyzer for in Situ Measurement of Soluble Reactive Phosphate: Improved Phosphate Blue Assay and Application to Fluvial Monitoring. *Environmental Science & Technology* **2017,** *51* (17), 9989-9995.
22. Plant, J. N.; Johnson, K. S.; Needoba, J. A.; Coletti, L. J., NH4-Digiscan: an in situ and laboratory ammonium analyzer for estuarine, coastal, and shelf waters. *Limnology and Oceanography: Methods* **2009,** *7* (2), 144-156.
23. Thouron, D.; Vuillemin, R.; Philippon, X.; Lourenço, A.; Provost, C.; Cruzado, A.; Garçon, V., An Autonomous Nutrient Analyzer for Oceanic Long-Term in Situ Biogeochemical Monitoring. *Analytical Chemistry* **2003,** *75* (11), 2601-2609.
24. Yucel, M.; Beaton, A. D.; Dengler, M.; Mowlem, M. C.; Sohl, F.; Sommer, S., Nitrate and Nitrite Variability at the Seafloor of an Oxygen Minimum Zone Revealed by a Novel Microfluidic In-Situ Chemical Sensor. *Plos One* **2015,** *10* (7), e0132785.
25. Coale, K. H.; Chin, C. S.; Massoth, G. J.; Johnson, K. S.; Baker, E. T., In situ chemical mapping of dissolved iron and manganese in hydrothermal plumes. *Nature* **1991,** *352*, 325.
26. Geißler, F.; Achterberg, E. P.; Beaton, A. D.; Hopwood, M. J.; Clarke, J. S.; Mutzberg, A.; Mowlem, M. C.; Connelly, D. P., Evaluation of a Ferrozine Based Autonomous in Situ Lab-on-Chip Analyzer for Dissolved Iron Species in Coastal Waters. *Frontiers in Marine Science* **2017,** *4* (322).
27. Vuillemin, R.; Le Roux, D.; Dorval, P.; Bucas, K.; Sudreau, J. P.; Hamon, M.; Le Gall, C.; Sarradin, P. M., CHEMINI: A new in situ CHEmical MINIaturized analyzer. *Deep Sea Research Part I: Oceanographic Research Papers* **2009,** *56* (8), 1391-1399.
28. Byrne, R. H., Measuring Ocean Acidification: New Technology for a New Era of Ocean Chemistry. *Environmental Science & Technology* **2014,** *48* (10), 5352-5360.
29. Song, H.; Chen, D. L.; Ismagilov, R. F., Reactions in Droplets in Microfluidic Channels. *Angewandte Chemie (International Ed.)* **2006,** *45* (44), 7336-7356.
30. Tice, J. D.; Song, H.; Lyon, A. D.; Ismagilov, R. F., Formation of Droplets and Mixing in Multiphase Microfluidics at Low Values of the Reynolds and the Capillary Numbers. *Langmuir* **2003,** *19* (22), 9127-9133.
31. Ogilvie, I. R. G.; Sieben, V. J.; Mowlem, M. C.; Morgan, H., Temporal Optimization of Microfluidic Colorimetric Sensors by Use of Multiplexed Stop-Flow Architecture. *Analytical Chemistry* **2011,** *83* (12), 4814-4821.
32. Song, H.; Tice, J. D.; Ismagilov, R. F., A Microfluidic System for Controlling Reaction Networks in Time. *Angewandte Chemie International Edition* **2003,** *42* (7), 768-772.
33. Hassan, S.; Nightingale, A. M.; Niu, X. Z., Continuous measurement of enzymatic kinetics in droplet flow for point-of-care monitoring. *Analyst* **2016,** *141* (11), 3266-3273.
34. Feng, S.; Shirani, E.; Inglis, W. D., Droplets for Sampling and Transport of Chemical Signals in Biosensing: A Review. *Biosensors* **2019,** *9* (2).
35. Pohl, G.; Shih, L. M., Principle and applications of digital PCR. *Expert Review of Molecular Diagnostics* **2004,** *4* (1), 41-47.
36. Zhang, Y. H.; Jiang, H. R., A review on continuous-flow microfluidic PCR in droplets: Advances, challenges and future. *Analytica Chimica Acta* **2016,** *914*, 7-16.
37. Brouzes, E.; Medkova, M.; Savenelli, N.; Marran, D.; Twardowski, M.; Hutchison, J. B.; Rothberg, J. M.; Link, D. R.; Perrimon, N.; Samuels, M. L., Droplet microfluidic technology for single-cell high-throughput screening. *Proceedings of the National Academy of Sciences of the United States of America* **2009,** *106* (34), 14195-14200.

38. Zhu, Z.; Yang, C. Y. J., Hydrogel Droplet Microfluidics for High-Throughput Single Molecule/Cell Analysis. *Accounts of Chemical Research* **2017,** *50* (1), 22-31.
39. Sesen, M.; Alan, T.; Neild, A., Droplet control technologies for microfluidic high throughput screening (mu HTS). *Lab on a Chip* **2017,** *17* (14), 2372-2394.
40. Athavale, R.; Pankratova, N.; Dinkel, C.; Bakker, E.; Wehrli, B.; Brand, A., Fast Potentiometric CO2 Sensor for High-Resolution in Situ Measurements in Fresh Water Systems. *Environmental Science & Technology* **2018,** *52* (19), 11259-11266.
41. Niu, X.; deMello, Andrew J., Building droplet-based microfluidic systems for biological analysis. *Biochemical Society Transactions* **2012,** *40* (4), 615-623.
42. Nightingale, A. M.; Evans, G. W. H.; Xu, P. X.; Kim, B. J.; Sammer-ul, H.; Niu, X. Z., Phased peristaltic micropumping for continuous sampling and hardcoded droplet generation. *Lab on a Chip* **2017,** *17* (6), 1149-1157.
43. Nightingale, A. M.; Leong, C. L.; Burnish, R. A.; Hassan, S.-u.; Zhang, Y.; Clough, G. F.; Boutelle, M. G.; Voegeli, D.; Niu, X., Monitoring biomolecule concentrations in tissue using a wearable droplet microfluidic-based sensor. *Nature Communications* **2019,** *10* (1), 2741.
44. Nightingale, A. M.; Hassan, S.-u.; Evans, G. W. H.; Coleman, S. M.; Niu, X., Nitrate measurement in droplet flow: gas-mediated crosstalk and correction. *Lab on a Chip* **2018,** *18* (13), 1903-1913.
45. Garcia-Robledo, E.; Corzo, A.; Papaspyrou, S., A fast and direct spectrophotometric method for the sequential determination of nitrate and nitrite at low concentrations in small volumes. *Marine Chemistry* **2014,** *162*, 30-36.
46. Miranda, K. M.; Espey, M. G.; Wink, D. A., A rapid, simple spectrophotometric method for simultaneous detection of nitrate and nitrite. *Nitric Oxide-Biology and Chemistry* **2001,** *5* (1), 62-71.
47. Schnetger, B.; Lehners, C., Determination of nitrate plus nitrite in small volume marine water samples using vanadium(III)chloride as a reduction agent. *Marine Chemistry* **2014,** *160*, 91-98.
48. Wang, S.; Lin, K. N.; Chen, N. W.; Yuan, D. X.; Ma, J., Automated determination of nitrate plus nitrite in aqueous samples with flow injection analysis using vanadium (III) chloride as reductant. *Talanta* **2016,** *146*, 744-748.
49. Hassan, S.-u.; Nightingale, A. M.; Niu, X., Micromachined optical flow cell for sensitive measurement of droplets in tubing. *Biomedical Microdevices* **2018,** *20* (4), 92.
50. Hassan, S.; Nightingale, A. M.; Niu, X. Z., Optical Flow Cell for Measuring Size, Velocity and Composition of Flowing Droplets. *Micromachines* **2017,** *8* (2), 58.
51. Beaton, A. D.; Sieben, V. J.; Floquet, C. F. A.; Waugh, E. M.; Abi Kaed Bey, S.; Ogilvie, I. R. G.; Mowlem, M. C.; Morgan, H., An automated microfluidic colourimetric sensor applied in situ to determine nitrite concentration. *Sensors and Actuators B: Chemical* **2011,** *156* (2), 1009-1014.
52. Schierenbeck, T. M.; Smith, M. C., Path to Impact for Autonomous Field Deployable Chemical Sensors: A Case Study of in Situ Nitrite Sensors. *Environmental Science & Technology* **2017,** *51* (9), 4755-4771.
53. Head, P. C., *Practical estuarine chemistry: a handbook*. 1 ed.; Cambridge University Press: 1985.
54. Loock, H.-P.; Wentzell, P. D., Detection limits of chemical sensors: Applications and misapplications. *Sensors and Actuators B: Chemical* **2012,** *173*, 157-163.
55. Edisbury, J. R., *Practical hints on absorption spectrometry (ultra-violet and visible)*. Hilger and Watts Ltd: 1966.
56. Yang, T.; Stavrakis, S.; deMello, A., A High-Sensitivity, Integrated Absorbance and Fluorescence Detection Scheme for Probing Picoliter-Volume Droplets in Segmented Flows. *Analytical Chemistry* **2017,** *89* (23), 12880-12887.
57. www.southamptonweather.co.uk (accessed June 2019).
58. Collins, M. B.; Ansell, K., *Solent Science - a review. Proceedings of Solent Science Conference, Southampton, 29 September 2000*. Elsevier Science: 2000; Vol. 1, p 385.

59. Veeck, L. Studies of nitrous oxide and the nitrogen cycle in a temperate river-estuarine system. Masters, University of Southampton, 2007.
60. Hydes, D. J.; Wright, P. N. *SONUS: The Southern Nutrients Study 1995-1997*; 1999.
61. www.sotonmet.co.uk (accessed June 2019).
62. Wade, A. J.; Palmer-Felgate, E. J.; Halliday, S. J.; Skeffington, R. A.; Loewenthal, M.; Jarvie, H. P.; Bowes, M. J.; Greenway, G. M.; Haswell, S. J.; Bell, I. M.; Joly, E.; Fallatah, A.; Neal, C.; Williams, R. J.; Gozzard, E.; Newman, J. R., Hydrochemical processes in lowland rivers: insights from in situ, high-resolution monitoring. *Hydrology and Earth System Sciences* **2012,** *16* (11), 4323-4342.

632

633 **TOC Art**

634